Journal of Alloys and Compounds 647 (2015) 123–128

Contents lists available at ScienceDirect

Journal of Alloys and Compounds

journal homepage: http://www.elsevier.com/locate/jalcom

# Study of photocatalytic activities of $Bi_2WO_6$ nanoparticles synthesized by fast microwave-assisted method

Nguyen Dang Phu [a], Luc Huy Hoang [a, *], Xiang-Bai Chen [b, **], Meng-Hong Kong [b], Hua-Chiang Wen [c], Wu Ching Chou [c]

[a] Faculty of Physics, Hanoi National University of Education, 136 Xuanthuy, Cau Giay, Hanoi, Viet Nam
[b] School of Science and Laboratory of Optical Information Technology, Wuhan Institute of Technology, Wuhan 430205, China
[c] Department of Electrophysics, National Chiao Tung University, Hsin-Chu 30010, Taiwan

ARTICLE INFO

*Article history:*
Received 15 March 2015
Received in revised form
3 June 2015
Accepted 5 June 2015
Available online 23 June 2015

*Keywords:*
Microwave-assisted synthesis
$Bi_2WO_6$ nanoparticles
Photocatalytic activity

ABSTRACT

We present a study of photocatalytic activities of $Bi_2WO_6$ nanoparticles synthesized by fast microwave-assisted method. The photocatalytic activities of the nanoparticles were evaluated by the decolorization of methylene-blue under visible-light-irradiation. Our results show that the surface area of $Bi_2WO_6$ nanoparticles plays a major role for improving photocatalytic activity, while visible-light absorption has only a weak effect on photocatalytic activity. This suggests efficient transportation of photo-generated electrons and holes to the oxidation active sites on the surface of nanoparticles, indicating $Bi_2WO_6$ nanoparticles synthesized by fast microwave-assisted method are promising for achieving high photocatalytic activity under visible-light-irradiation.



## 1. Introduction

Oxide-semiconductor-based photocatalysts have attracted extensive research attention for their potential applications in solar energy conversion and environmental pollutants treatment [1–4]. To date, $TiO_2$-based photocatalysts have been mostly studied due to their high oxidizability, good chemical stability, non-toxicity, and low cost [5–8]. However, $TiO_2$ can only be activated by ultraviolet light with wavelength shorter than 390 nm, which accounts for only 5% of the solar energy [9,10]. Therefore, it is essential to develop novel visible-light-induced photocatalyst with high efficiency under normal solar light condition. $Bi_2WO_6$, a typical aurivillius oxide with layered structure, has excellent intrinsic physical and chemical properties [11–13]. Recently, $Bi_2WO_6$-based photocatalysts have been widely studied for their promising photocatalytic performance under visible-light-irradiation [14–26]. Unfortunately, the electron–hole recombination in $Bi_2WO_6$ prohibits the desirable catalytic activity [27]. Therefore understanding how to improve the catalytic activity of $Bi_2WO_6$ nanomaterials would be important.

The typical processes in the treatment of pollutant by oxide-semiconductor-based photocatalysts are: (i) generation of electrons and holes by absorption of light, (ii) transportation of photo-generated electrons and holes to the active sites before recombination, and (iii) oxidation of the pollutant by the charges on active sites. One important factor affecting the generation of charges for oxidation would be crystalline quality. The higher the crystalline quality, the smaller is the amount of defects. The defects operate as trapping and recombination centers between photo-generated charges, resulting in a decrease in the photocatalytic activity. The number of active sites would be determined by the surface property of nanoparticles, such as surface area and vacancies on the surface. The surface area can be controlled by particle size, porosity distribution, etc. For instance, smaller size nanoparticles have bigger surface area, thus more active sites, that can lead to higher photocatalytic activity. The transportation efficiency of photo-generated charges to active sites would depend not only on intrinsic property of nanoparticles, but also on particle size distribution and how nanoparticles are assembled. When nanoparticles with different size are assembled close together, there would have charge transfer between different size nanoparticles. This would increase the transportation efficiency of photo-generated charges to active sites.

* Corresponding author.
** Corresponding author.
*E-mail addresses:* hoanglhsp@hnue.edu.vn (L.H. Hoang), xchen@wit.edu.cn (X.-B. Chen).

http://dx.doi.org/10.1016/j.jallcom.2015.06.047
0925-8388/

The transportation efficiency of photo-generated charges to active sites would be an important indicator to determine whether or not the photocatalyst is promising to achieve high catalytic activity. While, direct study of this issue would be difficult. In this paper, we investigate photocatalytic activity of $Bi_2WO_6$ nanoparticles with different crystalline quality, optical property, and particle size; then discuss our results in correlation with the transportation efficiency of photo-generated charges to the active sites. In a previous study of high photocatalytic activity $TiO_2$ nanoparticles, a linear dependence of the photocatalytic activity toward the degradation of MB on the photocatalyst surface area has been reported [28]. For the $Bi_2WO_6$ nanoparticles prepared by fast microwave-assisted method, a linear increase of photocatalytic activity with increasing surface area was also observed, indicating these nanoparticles are promising for achieving high photocatalytic activity.

## 2. Experimental

The $Bi_2WO_6$ nanoparticles were prepared by microwave-assisted method, which has the advantages of short reaction time, energy saving, highreaction rate, and easy form of complex oxides at relative low annealing temperature [29–32]. All the reagents, sodium tungstate dihydrate (Merck), bismuth nitrate (Merck) and methylene blue (SD Fine), were of analytical grade and used as received. In a typical synthesis, 2.5 mmol of sodium tungstate dihydrate ($Na_2WO_4.2H_2O$) and 5 mmol of bismuth nitrate ($Bi(NO_3)_3.5H_2O$) were first dissolved in 100 ml distilled water with 30 min stirring at room temperature. The obtained solution was heated by a Sanyo microwave oven with 500 W for 20 min. After microwave processing, the solution was cooled to room temperature. The resulted precipitate was separated by centrifugation, washed with deionized water and acetone for several times, then dried in an oven at 70 °C for 24 h. The samples were finally annealed in air for 5 h at temperatures of 400, 500, 600, and 700 °C, respectively.

The crystalline quality and phase purity of the products were investigated by an X-ray diffractometer (XRD, Bruker D5005). The morphology of the nanoparticles was observed by scanning electron microscope (SEM, S4800-Hitachi, secondary electrons were detected), the average particle size was statistics calculated by image J software. The layered structure of the nanoparticles was observed by high resolution transmission electron microscope (HRTEM, JEOL-2010 operated at 200 kV). The optical property of the nanoparticles was examined by UV–vis diffuse reflectance spectroscopy (UV–vis DRS, Jasco-V670). The BET surface area of the nanoparticles was determined using a Micromeritics Tristar 3000 V6.04 A.

Photocatalytic activity of the nanoparticles was evaluated by the decolorization of methylene-blue (MB) under visible-light-irradiation. In the experimental setup, a 300 W Xe lamp was employed as the light source and a 420 nm cut-off filter was used to provide visible-light-irradiation. In every experiment, 0.1 g of nanoparticles was added to 100 ml of MB solution ($10^{-5}$ mol/l). Before being irradiated, the suspension was magnetically stirred in the dark for 3 h to ensure the establishment of an adsorption–desorption equilibrium between the photocatalyst and MB. After a given irradiation time, the suspension was centrifuged to remove the catalyst immediately, and UV–VIS absorbance measurement was performed. The decolorization of MB was monitored by the decrease of absorption peaks.

For reusability test, the $Bi_2WO_6$ nanoparticles were immersed in ethanol for 3.0 h and rinsed with deionized water, and then dried at 370 K. After this, the cleaned $Bi_2WO_6$ nanoparticles were reused to test photocatalytic activity.

## 3. Results and discussion

Fig. 1 shows the XRD of the nanoparticles as-prepared and after annealing treatment at temperatures of 400, 500, 600, and 700 °C. The XRD results indicate that the nanoparticles as-prepared would be in *amorphous* state, thus yield no apparent diffraction peaks. With annealing treatment of 400 °C, $Bi_2WO_6$ can be formed with significant impurity phase of $Bi_{14}W_2O_{27}$. With annealing treatment above 500 °C, the crystalline quality of $Bi_2WO_6$ nanoparticles gets better, and the impurity $Bi_{14}W_2O_{27}$ phase disappears. The diffraction peaks of the nanoparticles obtained with annealing temperature above 500 °C can be well-indexed to pure orthorhombic $Bi_2WO_6$ phase according to the JCPDS Card (No.39-0256), as presented in Fig. 1. This indicates that good crystalline quality $Bi_2WO_6$ nanoparticles can be synthesized by fast microwave-assisted method with low temperature (500 °C) annealing treatment. With increasing annealing temperature, the linewidth of diffraction peaks gets sharper, indicating better crystalline quality $Bi_2WO_6$ nanoparticles can be obtained with higher annealing temperature. The decrease of linewidth also suggests an increase of nanoparticle grain size with increasing annealing temperature. Applying Scherrer equation to the (131) diffraction peak, the crystal grains of $Bi_2WO_6$ nanoparticles were estimated to be 20, 21, 26, and 31 nm for annealing temperatures of 400, 500, 600, and 700 °C, respectively.

For photocatalytic applications, better crystalline quality $Bi_2WO_6$ nanoparticles would results in more photo-generated charges for oxidation of pollutant, thus would be helpful for improving photocatalytic activity. To show better crystalline quality $Bi_2WO_6$ nanoparticles do have better optical property for potential improvement of photocatalytic activity, UV–VIS diffuse reflectance study is performed. Fig. 2(a) shows the UV–VIS diffuse reflectance spectra of the nanoparticles obtained with annealing temperatures of 400, 500, 600, and 700 °C. The intense absorption band with a steep edge is observed for all the samples, indicating that the visible-light absorption is mainly induced by intrinsic band-gap transitions instead of transitions from impurity levels [19]. According to the spectra, the samples present photo-absorption properties from UV to visible light shorter than 450 nm, which implied the possibility of good photocatalytic activity under visible-light-irradiation. For the $Bi_2WO_6$ nanoparticles obtained with annealing temperatures above 500 °C, the band-gap absorption gets steeper and stronger gradually with increasing annealing temperature. This indicates that the crystalline quality of the $Bi_2WO_6$ nanoparticles improves gradually with increasing annealing temperature, consistent with XRD results in Fig. 1.

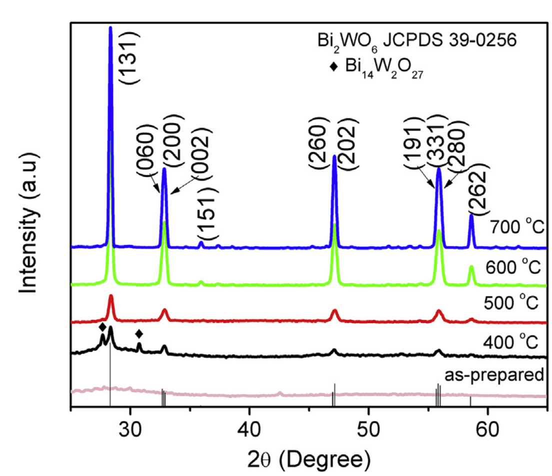


**Fig. 1.** XRD patterns of the nanoparticles as-prepared and after annealed at temperatures of 400, 500, 600, and 700 °C.

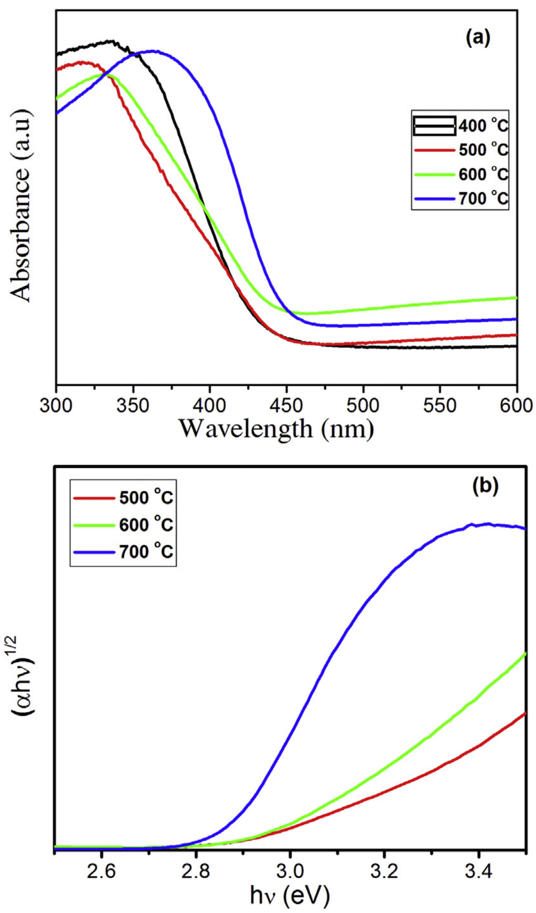


**Fig. 2.** (a) UV–VIS diffuse reflectance spectra of the nanoparticles obtained with annealing temperatures of 400, 500, 600, and 700 °C. (b) The relationships between $(\alpha h\nu)^{1/2}$ and photon energy of $Bi_2WO_6$ nanoparticles obtained with annealing temperatures of 500, 600, and 700 °C.

For the nanoparticles obtained with 400 °C annealing, the band-gap absorption is steeper and stronger than that of the $Bi_2WO_6$ nanoparticles obtained with 500 °C annealing. However, the XRD results show that the nanoparticles obtained with 400 °C annealing would have poor crystalline quality comparing with the $Bi_2WO_6$ nanoparticles obtained with 500 °C annealing. For the nanoparticles obtained with 400 °C annealing, the XRD pattern shows that there exists significant impurity phase of $Bi_{14}W_2O_{27}$ nanoparticles. Thus, the steep and strong band-gap absorption of the nanoparticles obtained with 400 °C annealing would be correlated with the optical absorption of $Bi_{14}W_2O_{27}$ nanoparticles. Therefore, if only optical absorption is concerned, both $Bi_2WO_6$ and $Bi_{14}W_2O_{27}$ nanoparticles could be potentially applied for visible-light-induced photocatalyst, and $Bi_{14}W_2O_{27}$ nanoparticles could be more promising than the $Bi_2WO_6$ nanoparticles.

It is well known that the optical absorption near the band edge for a crystalline semiconductor follows the formula $\alpha h\upsilon = A(h\upsilon - Eg)^{n/2}$, where $\alpha$, $h$, $\upsilon$, $Eg$, and $A$ are absorption coefficient, Planck constant, light frequency, band gap and a constant, respectively [15,18,19]. For direct band gap semiconductor $Bi_2WO_6$, n equals 1. The band gaps of the $Bi_2WO_6$ nanoparticles obtained with annealing temperature of 500, 600 and 700 °C were estimated to be 2.93, 2.89 and 2.83 eV, respectively, as shown in Fig. 2(b). For the nanoparticles obtained with 400 °C annealing, there are two phases of $Bi_2WO_6$ and $Bi_{14}W_2O_{27}$. These two phases would have different contribution for the absorption spectrum, thus the above formula could be not simply applied to one spectrum for obtaining the band gaps of two phases. Fig. 2(b) shows that the band gap decreases systematically with increasing annealing temperature. This indicates that bigger particle size $Bi_2WO_6$ nanoparticles were obtained with higher annealing temperature, consistent with XRD results.

Particle size and surface morphology are very important for improving photocatalytic activity of nanoparticles. To clearly observe the particle size and morphology of $Bi_2WO_6$ nanoparticles, SEM is performed, as shown in Fig. 3 (a–d). The increase of particle size with increasing annealing temperature is clearly observed in the SEM images. Using image J software, the average particle size of $Bi_2WO_6$ nanoparticles were found to be 30, 60, 80, and 400 nm for annealing temperatures of 400, 500, 600, and 700 °C, respectively. The particle sizes obtained from the SEM images are significantly larger than those estimated from XRD results. For the $Bi_2WO_6$ nanoparticles obtained with 700 °C annealing, the particle size obtained from SEM is more than 10 times of the particle size estimated from XRD. We suggest that this extreme difference would be mainly correlated with the layered structure of $Bi_2WO_6$ nanoparticles: the XRD results would mainly indicate the thickness of layered nanoparticles, while SEM images would mainly indicate the plane size of layered nanoparticles. The layered structure of the $Bi_2WO_6$ nanoparticles is confirmed by HRTEM image, as shown in Fig. 3(e). This image was taken for the $Bi_2WO_6$ nanoparticles obtained with annealing temperature of 500 °C. Fig. 3(e) shows that the average space between adjacent planes is 0.31 nm, which is assigned to the (131) planes of orthorhombic layered structure of $Bi_2WO_6$.

The surface areas of the $Bi_2WO_6$ nanoparticles were estimated by BET experiments, the results are shown in Table 1. With increasing annealing temperature, the particle surface area deceases gradually. For the $Bi_2WO_6$ nanoparticles obtained with annealing temperatures of 600 and 700 °C, their surface area is similar, although the SEM images indicated very different particle size. This further suggests that the SEM images indicated only the plane size of the layered nanoparticles. The thickness of the layered nanoparticles would be similar for the $Bi_2WO_6$ nanoparticles obtained with annealing temperatures of 600 and 700 °C, thus their surface areas are similar.

The above results show that with increasing annealing temperature, the crystalline quality of $Bi_2WO_6$ nanoparticles gets better, which improves the visible-light-absorption. This would result in more photo-generated electrons and holes, thus be helpful to improve photocatalytic activity. However, with increasing annealing temperature, the surface area of the $Bi_2WO_6$ nanoparticles gets smaller. This would result in less active sites, thus decrease the photocatalytic activity. Whether visible-light-absorption or surface-area plays major role for improving photocatalytic activity would depend on the efficiency of transportation of photo-generated charges to active sites. If surface area plays a major role, this would indicate high efficiency of transportation of photo-generated charges to active sites. Then, these nanoparticles would be promising for achieving high photocatalytic activity.

The photocatalytic activities of $Bi_2WO_6$ nanoparticles were tested by the decolorization of MB in an aqueous solution under visible-light-irradiation. Fig. 4 shows the temporal evolution of the UV–VIS spectra of MB solutions in the presence of $Bi_2WO_6$ nanoparticles (annealed at 500 °C) under visible light irradiation. With increasing irradiation time, the intensity of all the observed MB absorption peaks decreases. Besides, the absorption peak at 668 nm is blue-shifted and broadened. The blue-shifted absorption is characteristic of N-demethylated derivative(s) of MB [33]. This suggests decomposition of MB due to photocatalytic degradation process.

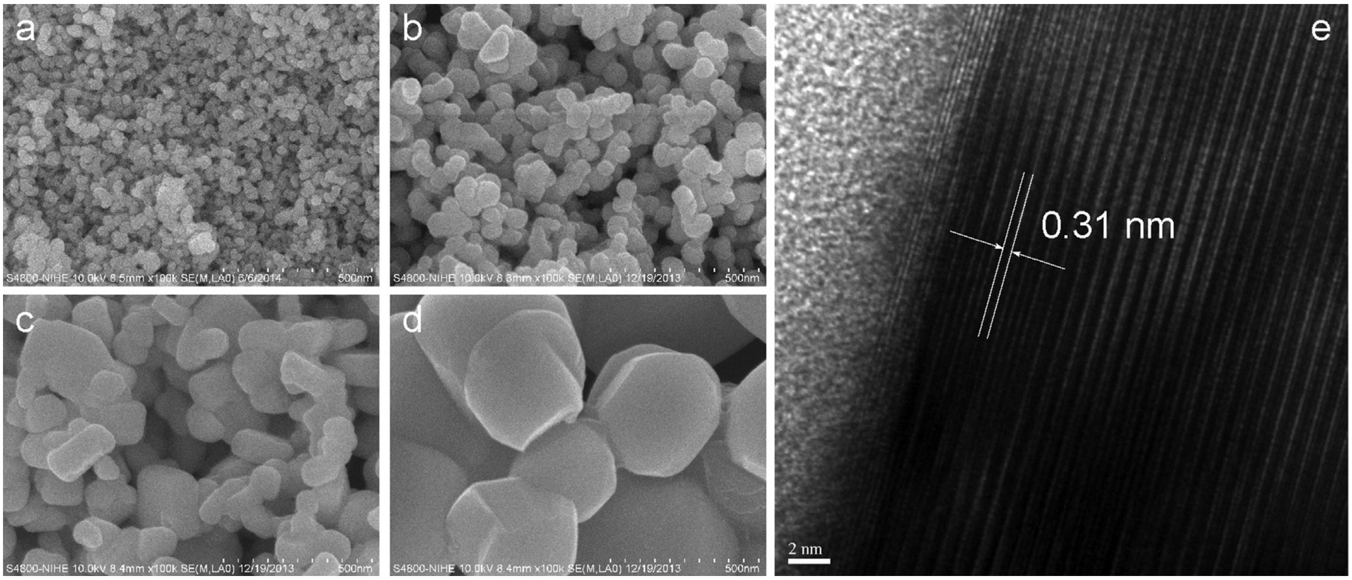


**Fig. 3.** SEM images of the nanoparticles obtained with annealing temperatures of 400 °C (a), 500 °C (b), 600 °C (c), 700 °C (d) and TEM image of $Bi_2WO_6$ nanoparticles obtained with annealing temperature of 500 °C (e).

**Table 1**
Surface areas of the $Bi_2WO_6$ nanoparticles obtained with annealing temperatures of 400, 500, 600, and 700 °C.

| Annealing temperature | 400 °C | 500 °C | 600 °C | 700 °C |
|---|---|---|---|---|
| Surface area ($m^2/g$) | 17.63 ± 0.04 | 14.60 ± 0.03 | 11.38 ± 0.03 | 10.63 ± 0.03 |

To compare the photocatalytic activities of the nanoparticles annealed at different temperatures. The absorbance time variations ($A_t/A_0$) of the peaks at 668 nm for nanoparticles annealed at 400, 500, 600, and 700 °C are plotted in Fig. 5 ($A_t$ is time-dependent absorbance and $A_0$ is initial absorbance). Fig. 5 shows that the nanoparticles obtained with annealing temperature of 400 °C have the lowest photocatalytic activity. This would be correlated with the significant impurity phase of $Bi_{14}W_2O_{27}$ nanoparticles. These nanoparticles have similar visible-light absorption with $Bi_2WO_6$ nanoparticles, and they have bigger surface area. Thus the low photocatalytic activity would indicate very low efficiency of transportation of photo-generated charges to active sites in $Bi_{14}W_2O_{29}$ nanoparticles. For the $Bi_2WO_6$ nanoparticles obtained with annealing temperature above 500 °C, the photocatalytic activity decreases gradually with increasing annealing temperature. We have shown that the visible-light absorption of the $Bi_2WO_6$ nanoparticles increases gradually with increasing annealing temperature; while the surface area of the nanoparticles decreases gradually with increasing annealing temperature. Thus, for the $Bi_2WO_6$ nanoparticles, the surface area plays more important role than visible-light absorption for enhancing photocatalytic activity. This indicates efficient transportation of photo-generated charges to active sites in the $Bi_2WO_6$ nanoparticles obtained with annealing at 500 °C.

Fig. 5 shows an important correlation between surface area and photocatalytic activity: the photocatalytic activity increases about

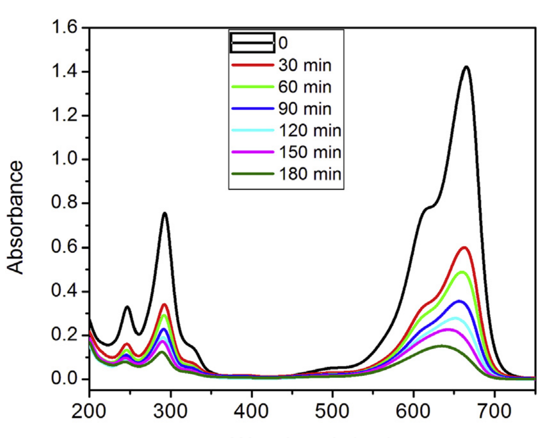


**Fig. 4.** Temporal evolution of the UV–VIS spectra of MB solutions in the presence of $Bi_2WO_6$ nanoparticles (annealed at 500 °C) under visible-light irradiation.

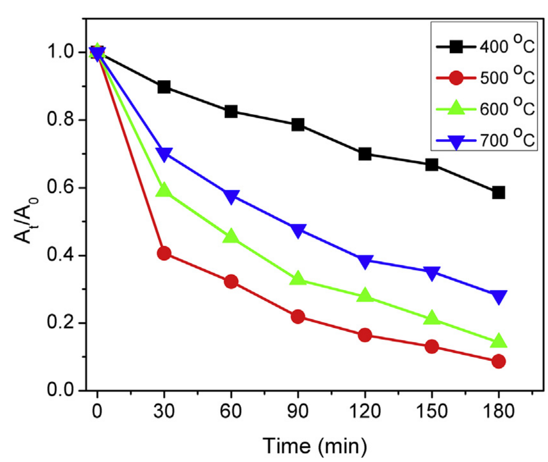


**Fig. 5.** Absorbance change of MB at 668 nm as a function of visible light irradiation time in the presence of $Bi_2WO_6$ nanoparticles annealed at different temperatures.

linearly about surface area of the $Bi_2WO_6$ nanoparticles. For $TiO_2$ nanoparticles, a linear dependence of photocatalytic activity toward the degradation of MB on the photocatalyst surface area was also reported [28]. Generally, $TiO_2$ nanoparticles have high efficiency of transportation of photo-generated charges to active sites. Thus the $Bi_2WO_6$ nanoparticles would be very promising for achieving high photocatalytic activity under visible-light-irradiation.

High efficiency of transportation of photo-generated charges to active sites would indicate very low recombination of free carriers, i.e., very low emission. Therefore, photoluminescence (PL) emission experiment is a useful technique to survey the separation efficiency of the photogenerated charge carriers in a semiconductor [34]. We have performed PL experiment on the $Bi_2WO_6$ nanoparticles obtained with annealing at 500 °C using 325 nm laser, no emission was detected. This further indicates the high efficiency of transportation of photo-generated charges to active sites in these $Bi_2WO_6$ nanoparticles. The high efficiency of transportation of photo-generated charges to active sites in these $Bi_2WO_6$ nanoparticles may be correlated the layered structure and disperse particle size distribution. The layered structure makes the nanoparticles like to stick together thus increase the probability of charge transfer between different size nanoparticles. Also, the disperse particle size distribution would increase the separation of electrons and holes into different size nanoparticles. These two factors would significantly decrease the high efficiency of electron–hole recombination in $Bi_2WO_6$ crystal, thus increase the efficiency of transportation of photo-generated charges to active sites on the surface of $Bi_2WO_6$ nanoparticles.

Considering practical application, it is important and necessary to investigate the reusability and stability of a photocatalyst. To confirm the reusability and stability of the photocatalytic performance of the $Bi_2WO_6$ nanoparticles, circulating runs in the photocatalytic degradation of MB under visible-light irradiation were checked. As shown in Fig. 6, comparing with the first run, the photocatalytic activity losses ~5%, 6%, and 10% for second, third, and fourth run, respectively.

We have discussed above that the $Bi_2WO_6$ nanoparticles synthesized by fast microwave-assisted method are promising candidate of visible-light-induced photocatalyst. To further improve the photocatalytic activity of these nanoparticles, following future studies would be helpful. (1) Improve visible-light absorption above 450 nm. This could be achieved by dope the $Bi_2WO_6$ nanoparticles [9]. (2) Increase the active sites on the surface of nanoparticles. This could be achieved by further controlling the synthesizing conditions to reduce particle size, or to obtain hollow sphere nanoparticles [22,35], flower-like nanostructures [36,37], or encapsulate $Bi_2WO_6$ nanoparticles into mesoporous structures [38], and so forth. Also, rough particle surface with more oxygen defect states may be helpful to increase the active sites on the surface [39]. (3) Increase the efficiency of transportation of photo-generated charges to active sites. This could be achieved by mixing $Bi_2WO_6$ nanoparticles with other semiconductor nanoparticles to separate electrons and holes more efficiently [40]. In our future studies, we will perform systematic studies of the above possibilities to further increase the photocatalytic activity of $Bi_2WO_6$ nanoparticles for their practical applications.

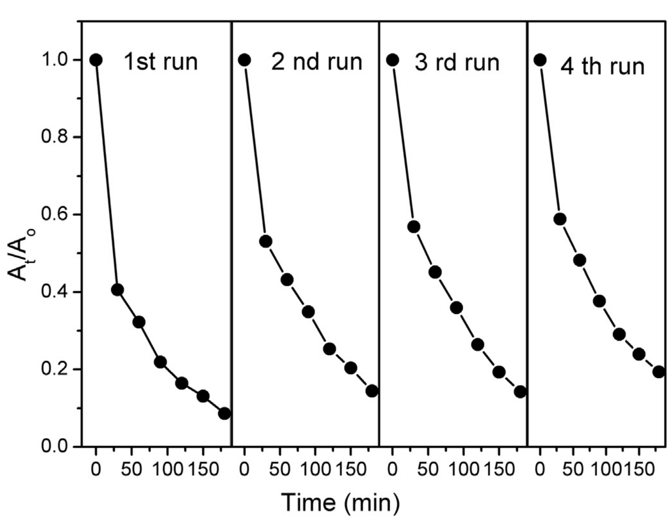


**Fig. 6.** Cycling runs of the photocatalytic degradation of MB under visible light in the presence of $Bi_2WO_6$ nanoparticles annealed at 500 °C.

## 4. Conclusions

The photocatalytic activities of $Bi_2WO_6$ nanoparticles synthesized via fast microwave-assisted method were studies by testing the decolorization of methylene-blue under visible-light-irradiation. The comparison of crystalline quality and surface area of the nanoparticles for enhancing photocatalytic activities are investigated. Our results indicated that surface area of the nanoparticles plays major role for increasing photocatalytic activity: the photocatalytic activities increases about linearly with increasing particle surface area; but weakly affected by crystal quality. This suggested high efficiency of transportation of photo-generated electrons and holes to the active sites before recombination, indicating $Bi_2WO_6$ nanoparticles synthesized by fast microwave-assisted method are promising for achieving high photocatalytic activity.

## Acknowledgements

The authors would like to thank the Vietnam's National Foundation for Science and Technology Development (NAFOSTED), grant 103.02-2013.51 for financial support. X. B. Chen acknowledges the support by Wuhan Institute of Technology.

## References

[1] Z. Zou, J. Ye, K. Sayama, H. Arakawa, Nature 414 (2001) 625–627.
[2] I.K. Konstantinou, T.A. Albanis, Appl. Catal. B: Environ. 49 (2004) 1–14.
[3] H.Q. Li, Y.M. Cui, W.S. Hong, Appl. Surf. Sci. 264 (2013) 581–588.
[4] M. Xie, Y. Feng, X. Fu, P. Luan, L. Jing, J. Alloys Compd. 631 (2015) 120–124.
[5] M.J. Esswein, D.G. Nocera, Chem. Rev. 107 (2007) 4022–4047.
[6] X. Chen, S.S. Mao, Chem. Rev. 107 (2007) 2891–2959.
[7] J.N. Schrauben, R. Hayoun, C.N. Valdez, M. Braten, L. Fridley, J.M. Mayer, Science 336 (2012) 1298–1301.
[8] Q.J. Liu, Z. Ran, F.S. Liu, Z.T. Liu, J. Alloys Compd. 631 (2015) 192–201.
[9] A.L. Linsebigler, G. Lu, J.T. Yates, Chem. Rev. 95 (1995) 735–758.
[10] J. Le, Y. Chen, F. Shen, L. Wang, Y. Liu, J. Zhang, J. Alloys Compd. 631 (2015) 328–334.
[11] Y. Shi, S. Feng, C. Cao, Mater. Lett. 44 (2000) 215–218.
[12] P. Ju, P. Wang, B. Li, H. Fan, S. Ai, D. Zhang, Y. Wang, Chem. Eng. J. 236 (2014) 430–437.
[13] M. Tachibana, Solid State Commun. 211 (2015) 1–3.
[14] J.W. Tang, Z.G. Zou, J.H. Ye, Catal. Lett. 92 (2004) 53–56.
[15] H.B. Fu, C.S. Pan, W.Q. Yao, Y.F. Zhu, J. Phys. Chem. B 109 (2005) 22432–22439.
[16] J. Li, X. Zhang, Z. Ai, F. Jia, L. Zhang, J. Lin. J. Phys. Chem. C 111 (2007) 6832–6836.
[17] D.X. Wu, H.T. Zhu, C.Y. Zhang, L. Chen, Chem. Commun. 46 (2010) 7250–7252.
[18] G. Zhao, S. Liu, Q. Lu, F. Xu, H. Sun, J. Alloys Compd. 578 (2013) 12–16.
[19] M. Shang, W. Wang, J. Ren, S. Sun, L. Wang, L. Zhang, J. Mater. Chem. 19 (2009) 6213–6218.
[20] F. Amano, K. Nogami, B. Ohtani, J. Phys. Chem. C 113 (2009) 1536–1542.
[21] D. Ma, S. Huang, W. Chen, S. Hu, F. Shi, K. Fan, J. Phys. Chem. C 113 (2009) 4369–4374.
[22] Y. Huang, Z. Ai, W. Ho, M. Chen, S. Lee, J. Phys. Chem. C 114 (2010) 6342–6349.
[23] S.P. Hua, C.Y. Xu, L. Zhen, Mater. Lett. 95 (2013) 117–120.
[24] X. Wang, P. Tian, Y. Lin, L. Li, J. Alloys Compd. 620 (2015) 228–232.
[25] G. Zhao, S. Liu, Q. Lu, F. Xu, H. Sun, J. Alloys Compd. 578 (2013) 12–16.

[26] E.P. Kharitonova, D.A. Belov, A.B. Gagor, A.P. Pietraszko, O.A. Alekseeva, V.I. Voronkova, J. Alloys Compd. 591 (2014) 308–314.
[27] M.S. Gui, W.D. Zhang, Q.X. Su, C.H. Chen, J. Solids State Chem. 184 (2011) 1977–1982.
[28] D. Meroni, V. Pifferi, B. Sironi, G. Cappelletti, L. Falciola, G. Cerrato, S. Ardizzone, J. Nanopart. Res. 14 (2012) 1086.
[29] S.E. Ela, S. Cogal, S. Icli, Inorg. Chim. Acta 362 (2009) 1855.
[30] T. Krishnakumar, R. Jayaprakash, N. Pinna, V.N. Singh, B.R. Mehta, A.R. Phani, Mater. Lett. 63 (2009) 242.
[31] L.H. Hoang, P.V. Hai, N.H. Hai, P.V. Vinh, X.B. Chen, I.S. Yang, Mater. Lett. 64 (2010) 962–965.
[32] P.V. Hanh, L.H. Hoang, P.V. Hai, N.V. Minh, X.B. Chen, I.S. Yang, J. Phys. Chem. Solids 74 (2013) 426–430.
[33] T.Y. Zhang, T. Oyama, A. Aoshima, H. Hidaka, J.C. Zhao, N. Serpone, J. Photochem. Photobiol. A 140 (2001) 163–172.
[34] J.W. Tang, Z.G. Zou, J.H. Ye, J. Phys. Chem. B 107 (2003) 14265–14269.
[35] X.J. Dai, Y.S. Luo, W.D. Zhang, S.Y. Fu, Dalton Trans. 39 (2010) 3426–3432.
[36] L.S. Zhang, W.Z. Wang, Z.G. Chen, L. Zhou, J. Mater. Chem. 17 (2007) 2526–2532.
[37] S.W. Liu, J.G. Yu, J. Solid State Chem. 181 (2008) 1048–1055.
[38] L.H. Hoang, P.V. Hanh, N.D. Phu, X.B. Chen, W.C. Chou, J. Phys. Chem. Solids 77 (2015) 122–125.
[39] L. Wu, J. Bi, Z. Li, X. Wang, X. Fu, Catal. Today 131 (2008) 15–20.
[40] Z.Q. Li, X.T. Chen, Z.L. Xue, J Colloid Interface Sci. 394 (2013) 69–77.